

Achieving High Performances of Nondoped OLEDs Using Carbazole and Diphenylphosphoryl-Functionalized Ir(III) Complexes as Active Components

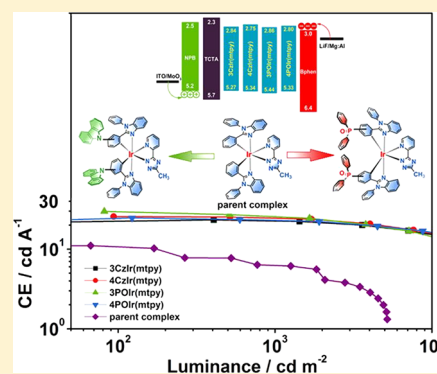
Hui-Ting Mao,[†] Chun-Xiu Zang,[‡] Guo-Gang Shan,^{*,†} Hai-Zhu Sun,[†] Wen-Fa Xie,^{*,‡} and Zhong-Min Su^{*,†}

[†]Institute of Functional Material Chemistry and National & Local United Engineering Lab for Power Battery, Faculty of Chemistry, Northeast Normal University, Changchun, Jilin 130024, P. R. China

[‡]State Key Laboratory on Integrated Optoelectronics, College of Electronic Science and Engineering, Jilin University, Changchun, Jilin 130012, P. R. China

Supporting Information

ABSTRACT: Nondoped electroluminescent devices offer advantages over their doped counterparts such as good reproducibility, reduced phase separation between host and guest materials, and potential of lower-cost devices. However, low luminance efficiencies and significant roll-off values are longstanding issues for nondoped devices, and a rational design strategy for the preparation of efficient phosphors is highly desired. In this work, cyclometalated Ir(III) complexes **3CzIr(mtpy)**, **4CzIr(mtpy)**, **3POIr(mtpy)**, and **4POIr(mtpy)** bearing carbazole (Cz) or diphenylphosphoryl (Ph_2PO) groups substituted at different positions of 1,2-diphenyl-*H*-benzimidazole (HPBI) were designed and synthesized. Owing to the steric effects induced by these groups, a significant intermolecular interaction was avoided, thereby reducing self-quenching and triplet–triplet annihilation (TTA) at high brightness. Simultaneously, attached functional moieties manipulate the charge-carrier character and enhance the EL performance of the complexes. Device **N3-10**, based on **3POIr(mtpy)**, successfully realized excellent performance and improved efficiency stability, rendering a turn-on voltage of 2.5 V, a maximum current efficiency of 29.7 cd A^{-1} , and a maximum power efficiency of 31.1 lm W^{-1} , which are all almost 3-fold higher than that of the control device **N-10** based on parent complex. Inspiringly, all of the devices showed reduced efficiency roll-off as luminance increased. To the best of our knowledge, these are good results for green-emitting PHOLEDs using vacuum evaporation techniques, and they provide fundamental insights into the future realization of efficient phosphorescent Ir(III) complexes and corresponding nondoped devices.



INTRODUCTION

Owing to the electron spin–orbit coupling (SOC) and fast intersystem crossing (ISC), phosphorescent transition-metal complexes provide high electroluminescence (EL) efficiencies by utilizing all singlet and triplet excitons to achieve internal quantum efficiencies (IQEs) of nearly 100%.¹ Phosphorescent OLEDs (PHOLEDs) show a better future as the potential candidates for full-color flat-panel displays and efficient solid-state lighting. In particular, cyclometalated iridium(III) complexes are considered to be the most promising phosphorescent dyes due to their merits of a high quantum yield and a relatively short excited-state lifetime as well as flexibility in color tuning, and thermal and electrochemical stability.^{1,2} Also, its ambipolar character, with oxidation mainly involving the metal and reduction mainly involving the coordinating ligands, allows the charge recombination to occur on the metal complex with formation of a luminescent excited state.³ However, luminescence self-quenching in the solid state and poor charge-transport capability significantly

limit the performance of devices for practical applications.^{2b,4} Consequently, phosphorescent emitters normally have to be blended into suitable host materials to keep the emissive chromophores separated, thus reducing the concentration quenching and/or triplet–triplet annihilation (TTA).^{2b,4} Nevertheless, host–guest systems have a few obstacles in their commercialization, such as phase separation upon heating and accurate control of doping concentration, despite improved EL efficiency.⁵ Alternatively, nondoped devices are more attractive because they are easier to employ for the preparation of reliable and reproducible commercial devices.⁶

To date, many efforts have been made to design iridium(III) dyes to fabricate efficient nondoped phosphorescent devices. In 2012, the Lai group synthesized phenanthroimidazole derivatives TPA-BPI, with a structure of donor–linker–acceptor, and deep-blue emitters were obtained.⁷ The resulting nondoped

Received: June 14, 2017

devices exhibited excellent performance, accompanied by a favorable current efficiency up to 2.63 cd A^{-1} and an external quantum efficiency up to 3.08%. Wang and co-workers reported that an amidinate-ligated iridium(III) bis(2-pyridyl)phenyl complex, which endowed the nondoped device with a rather low turn-on voltage (2.3 cd m^{-2} at 2.4 V) and a respectable power efficiency as high as 32.5 lm W^{-1} , which is superior to some reported iridium(III)-based doped devices.⁸ Recently, our group and others have demonstrated that 1,2-diphenyl-*H*-benzimidazole (HPBI) could serve as an excellent cyclometalated ligand for phosphorescent iridium(III) complexes, giving rise to significant enhancement of the emitting properties such as improved nondoped EL efficiency.⁹ More importantly, the nondoped devices exhibit reduced efficiency roll-offs at higher brightnesses. We chose 2-(3-methyl-1*H*-1,2,4-triazol-5-yl)pyridine (mtpy) as an ancillary ligand because of the deprotonation of the azole ring upon coordination, leading to a neutral iridium complex. It also indicates that the introduction of small substituents to HPBI ligands, such as methyl and *tert*-butyl moieties, results in much more efficient heteroleptic iridium(III) complexes, which achieve higher EL performances and improved efficiency stability compared to that of the parent complex.¹⁰ From a chemical structure standpoint, such small alkyl groups should have little effect on their charge-transporting abilities, although the charge-transporting ability is crucial to the EL efficiency, in particular for nondoped devices. Therefore, it is believed that EL performances can be further enhanced if the charge-transporting abilities of employed materials are modified judiciously.

Recent reports have shown that the charge injection and transporting characters for phosphorescent dyes could be modified through the integration of functional moieties, for instance, main-group moieties.¹¹ Moreover, it should be considered that attaching functional units on the phosphorescent emitters as steric hindrance could efficiently suppress intermolecular interaction and hence, reduce self-quenching effects, making them impressive as phosphorescent dyes for high-performance nondoped PhOLEDs.^{11a,12} Therefore, there is much room to design efficient phosphors with HPBI ligands for high-performance nondoped devices by molecular engineering. To prove this concept, we attempt to simultaneously attach relatively large functional units on HPBI ligand as steric hindrance and manipulate its charge-transporting abilities.

On the basis of the above considerations, herein, carbazole (Cz) and diphenylphosphoryl (Ph_2PO) groups are incorporated into different positions of the HPBI ligands to design a class of phosphorescent iridium complexes, namely $3\text{CzIr}(\text{mtpy})$, $4\text{CzIr}(\text{mtpy})$, $3\text{POIr}(\text{mtpy})$, and $4\text{POIr}(\text{mtpy})$ (see Figure 1). As the steric hindrance units, Cz and Ph_2PO effectively suppressed intermolecular interactions between the emissive Ir cores and manipulated their charge-carrier characters. In addition, the parent complex $(\text{pbi})_2\text{Ir}(\text{mtpy})$ was also prepared for the control device. Consequently, these functional complexes, with favorable charge mobilities, realize the yellow-green emission at 511, 504, 498, and 523 nm, respectively. High-performance nondoped devices based on functionalized iridium(III) complexes are obtained, achieving improved EL efficiencies and lower efficiency roll-off than that of the parent-complex-based device. For example, the nondoped device using $3\text{POIr}(\text{mtpy})$ as the emitting layer exhibits outstanding performance with a maximum current efficiency (CE) of 29.7 cd A^{-1} and a maximum power efficiency (PE) of

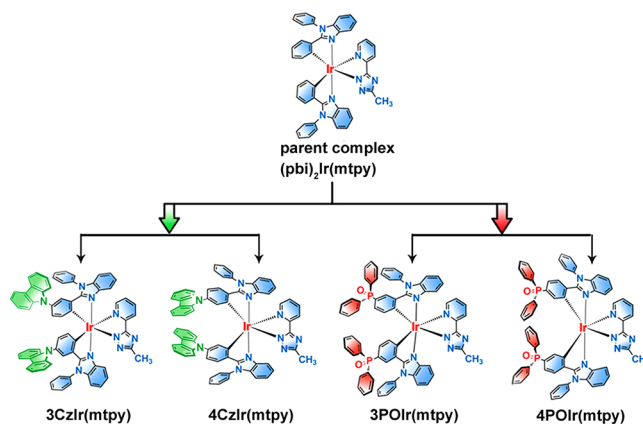


Figure 1. Chemical structures of $(\text{pbi})_2\text{Ir}(\text{mtpy})$, $3\text{CzIr}(\text{mtpy})$, $4\text{CzIr}(\text{mtpy})$, $3\text{POIr}(\text{mtpy})$, and $4\text{POIr}(\text{mtpy})$.

31.1 lm W^{-1} , which is 3-fold higher compared to that of the reference device (11.1 cd A^{-1} , 11.6 lm W^{-1}).

EXPERIMENTAL SECTION

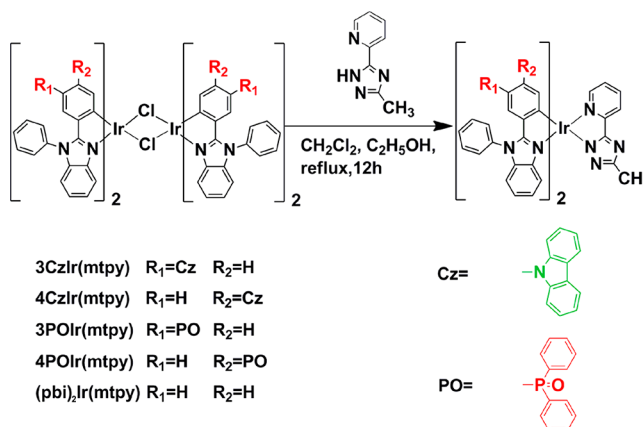
General Information. All reagents and solvents used for the experiment were purchased from commercial sources. All solvents for chemical synthesis were dried and distilled from appropriate drying agents prior to use. The experiments were prepared under a nitrogen atmosphere. ^1H NMR spectra were recorded with a Bruker Avance 500 MHz spectrometer, and chemical shifts are reported with tetramethylsilane (TMS) as the internal standard. An electrospray ionization mass spectrometer was used to record mass spectra for these complexes. The high-resolution mass spectral (HRMS) analysis was recorded on Bruker Daltonics flex Analysis. Elemental analyses were performed on a Perkin-Elmer 240C elemental analyzer.

Synthesis of Ligands. 9-(3-(1-phenyl-1*H*-benzimidazol-2-yl)phenyl)-9*H*-carbazole (3CzPBI), 9-(4-(1-phenyl-1*H*-benzimidazol-2-yl)phenyl)-9*H*-carbazole (4CzPBI), diphenyl(3-(1-phenyl-1*H*-benzimidazol-2-yl)phenyl)phosphine oxide (3POPBI), diphenyl(4-(1-phenyl-1*H*-benzimidazol-2-yl)phenyl)phosphine oxide (4POPBI) (see Scheme S1),^{9b,13} and 2-(3-methyl-1*H*-1,2,4-triazol-5-yl)pyridine (mtpy) were conveniently synthesized according to early reports.¹⁴ These complexes were prepared according to our previous reports.^{9a,d}

Synthesis of Iridium(III) Complexes. See Scheme 1 for a schematic describing the synthesis of the iridium(III) complexes.

$3\text{CzIr}(\text{mtpy})$. A mixture of $\text{IrCl}_3 \cdot 3\text{H}_2\text{O}$ (0.35 g, 1.00 mmol) and 3CzPBI (0.95 g, 2.20 mmol) in 2-ethoxyethanol and water (3:1, v/v) was refluxed for 24 h under argon. Then, the reaction mixture was cooled down to room temperature. After filtered, the residue was washed with water (30 mL) and ethanol (30 mL). The μ -chloro-

Scheme 1. Synthetic Routes of Iridium(III) Complexes



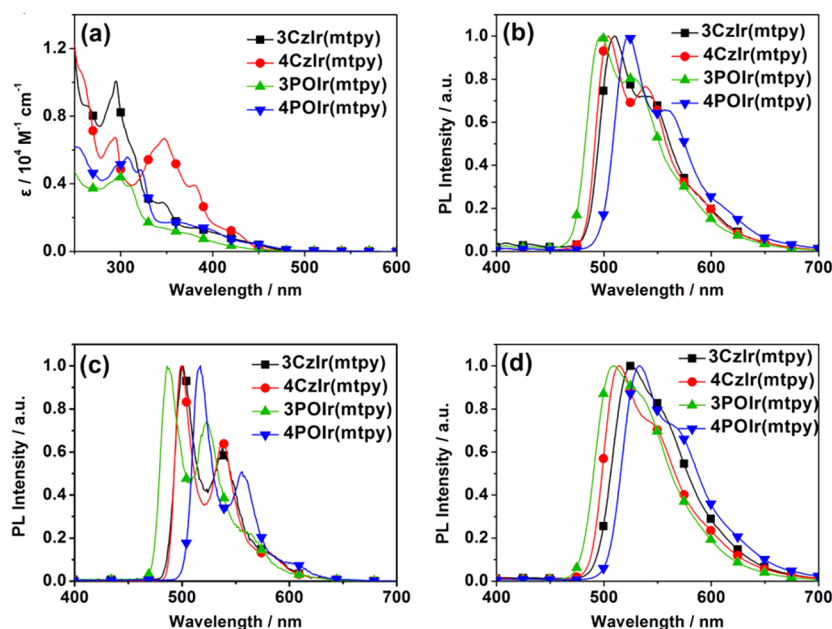


Figure 2. (a) UV-vis absorption spectra of the complexes in CH₂Cl₂ (10⁻⁵ M). (b) PL spectra at 298 K. (c) PL spectra at 77 K. (d) PL spectra of iridium complexes in neat film.

bridged dimer complex (0.64 g, 0.29 mmol), [Ir(3CzPBI)₂Cl]₂, was collected without further purification after it was dried out. A solution of **mtpy** (0.07 g, 0.45 mmol) and the μ -chloro-bridged dimer complex [Ir(3CzPBI)₂Cl]₂ (0.40 g, 0.18 mmol) in CH₂Cl₂ (30 mL) and ethanol (10 mL) was refluxed for 12 h under argon in the dark. After cooling to room temperature, the mixture was filtered. The crude product was purified by silica gel column chromatography (eluent: ethyl acetate/dichloromethane = 1:1, v/v) to afford white powder in 63% yield (0.27 g, 0.23 mmol). ¹H NMR (500 MHz, CDCl₃, δ [ppm]): 8.15 (d, *J* = 7.5 Hz, 4H), 8.08–8.12 (m, 2H), 7.77–7.81 (m, 4H), 7.65–7.73 (m, 3H), 7.55–7.59 (m, 2H), 7.45–7.48 (m, 2H), 7.39 (t, *J* = 7.0 Hz, 4H), 7.20–7.31 (m, 11H), 7.11–7.18 (m, 4H), 7.07–7.10 (m, 2H), 6.84–6.88 (m, 4H), 6.28 (d, *J* = 8.0 Hz, 1H), 5.93 (d, *J* = 8.0 Hz, 1H), 2.40 (s, 3H). MS [*m/z*]: Calcd for C₇₀H₄₇IrN₁₀ 1220.4, Found 1221.4 (M + H⁺). Anal. Calcd for C₇₀H₄₇IrN₁₀: C, 68.89; H, 3.88; N, 11.48. Found: C, 68.93; H, 3.82; N, 11.39.

4CzIr(mtpy). According to the above-mentioned typical procedure, the main ligand 3CzPBI of 3CzIr(mtpy) was replaced by 4CzPBI. The crude product was purified by silica gel column chromatography (eluent: ethyl acetate/dichloromethane = 1:1, v/v) to afford white powder in 67% yield (0.29 g, 0.24 mmol). ¹H NMR (500 MHz, CDCl₃, δ [ppm]): 8.23 (d, *J* = 5.0 Hz, 1H), 8.11–8.13 (m, 5H), 8.07 (d, *J* = 7.5 Hz, 1H), 7.81–7.84 (m, 1H), 7.75–7.77 (m, 4H), 7.65–7.71 (m, 3H), 7.56 (s, 1H), 7.18–7.20 (m, 12H), 7.11–7.17 (m, 5H), 7.02–7.08 (m, 3H), 6.93–6.95 (m, 2H), 6.88 (d, *J* = 8.5 Hz, 2H), 6.77–6.79 (m, 2H), 6.25 (d, *J* = 8.0 Hz, 1H), 5.91 (d, *J* = 8.5 Hz, 1H), 2.39 (s, 3H). MS [*m/z*]: Calcd for C₇₀H₄₇IrN₁₀ 1220.4, Found 1221.4 (M + H⁺). Anal. Calcd for C₇₀H₄₇IrN₁₀: C, 68.89; H, 3.88; N, 11.48. Found: C, 68.87; H, 3.86; N, 11.51.

3POIr(mtpy). According to the above-mentioned typical procedure, the main ligand 3CzPBI of 3CzIr(mtpy) was replaced by 3POPBI. The crude product was also purified by silica gel column chromatography (eluent: methanol/dichloromethane = 1:20, v/v) to afford white powder in 53% yield (0.23 g, 0.18 mmol). ¹H NMR (500 MHz, CDCl₃, δ [ppm]): 8.01–8.09 (m, 2H), 7.81 (d, *J* = 5.5 Hz, 1H), 7.47–7.60 (m, 11H), 7.38–7.46 (m, 13H), 7.36–7.37 (m, 8H), 7.21–7.24 (m, 2H), 6.97–7.06 (m, 4H), 6.90–6.92 (m, 1H), 6.81–6.88 (m, 1H), 6.70–6.78 (m, 2H), 6.62–6.64 (m, 1H), 6.09 (d, *J* = 8.5 Hz, 1H), 5.77 (d, *J* = 8.5 Hz, 1H), 2.32 (s, 3H). MS [*m/z*]: Calcd for C₇₀H₅₁IrN₈O₂P₂ 1290.3, Found 1291.3 (M + H⁺). Anal. Calcd for C₇₀H₅₁IrN₈O₂P₂: C, 65.16; H, 3.98; N, 8.68. Found: C, 65.18; H, 4.03; N, 8.72.

4POIr(mtpy). According to the above-mentioned typical procedure, the main ligand 3CzPBI of 3CzIr(mtpy) was replaced by 4POPBI. The crude product was also purified by silica gel column chromatography (eluent: methanol/dichloromethane = 1:15, v/v) and then methanol/dichloromethane = 1:10, v/v) to afford white powder in 58% yield (0.25 g, 0.20 mmol). ¹H NMR (500 MHz, CDCl₃, δ [ppm]): 8.09 (t, *J* = 7.5 Hz, 1H), 8.03 (d, *J* = 7.0 Hz, 1H), 7.87 (d, *J* = 5.5 Hz, 1H), 7.77–7.81 (m, 2H), 7.74 (s, 3H), 7.71–7.72 (m, 1H), 7.63–7.67 (m, 2H), 7.40–7.46 (m, 5H), 7.26–7.29 (m, 3H), 7.21–7.24 (m, 7H), 7.15–7.18 (m, 2H), 7.10–7.14 (m, 2H), 7.03–7.08 (m, 4H), 6.70–7.01 (m, 2H), 6.95–6.98 (m, 2H), 6.88–6.92 (m, 2H), 6.77 (d, *J* = 8.5 Hz, 1H), 6.64 (d, *J* = 8.0 Hz, 1H), 6.53–6.59 (m, 4H), 6.06 (d, *J* = 7.0 Hz, 1H), 5.71 (d, *J* = 8.5 Hz, 1H), 2.32 (s, 3H). MS [*m/z*]: Calcd for C₇₀H₅₁IrN₈O₂P₂ 1290.3, Found 1291.3 (M + H⁺). Anal. Calcd for C₇₀H₅₁IrN₈O₂P₂: C, 65.16; H, 3.98; N, 8.68. Found: C, 65.08; H, 3.88; N, 8.62.

Physical Measurements. UV-vis absorption spectra were measured on Cary 500 UV-vis-NIR spectrophotometer. The photoluminescence (PL) spectra of these complexes were reported on the FL-4600 FL spectrophotometer. The excited-state lifetimes (τ) and Φ_p in solution were measured on a transient spectrofluorimeter (Edinburgh FLSP920) using a time-correlated single-photon counting system. The luminescence quantum efficiencies (Φ_p) in neat films were measured in an integrating sphere. Emission spectra were recorded using the F-7000 FL spectrophotometer.

Theoretical Calculations. The calculations reported here were carried out by using the Gaussian 09 software package.¹⁵ The geometrical structures of the singlet ground state and the lowest triplet state for iridium(III) complexes were fully optimized with C1 symmetry constraints by using the restricted closed-shell and open-shell PBE1PBE methods with the LANL2DZ basis set for the Ir atom and 6-31G* for the rest of the atoms.¹⁶ The effective core potential on Ir replaced the inner-core electrons, leaving the outer core (5s)²(5p)⁶ electrons and the (5d)⁶ valence electrons of iridium(III).¹⁷ On the basis of the optimized S₀, Tamm–Dancoff Approximation (TDA) in time-dependent DFT (TD-DFT) calculations were performed in order to determine the vertical transition characters and simulate the UV-vis absorption property simultaneously.¹⁸ The solvent effect was also considered with the polarized continuum model.

Electrochemical Measurements. Cyclic voltammetry (CV) measurements were carried out with a BAS 100 W instrument with a scan rate of 100 mV s⁻¹ in CH₂Cl₂ (10⁻³ M) with three electrode

Table 1. Photophysical and Electrochemical Characteristics of Iridium(III) Complexes

complexes	$\lambda_{\text{PL,max}}^{a,b,c}$ (nm)	$\Phi^{a,c}$ (%)	$\tau^{a,c}$ (μs)	E_{g}^{d} (eV)	E_{ox}^e (V)	HOMO ^f (eV)	LUMO ^g (eV)
(pbi) ₂ Ir(mtpy)	501, 493, 520	48, 24	0.33, 0.19	2.67	0.83	-5.15	-2.48
3CzIr(mtpy)	511, 500, 525	12.7, 10.3	0.38, 0.28	2.43	0.47	-5.27	-2.84
4CzIr(mtpy)	504, 500, 515	10.3, 52.8	0.87, 0.48	2.59	0.54	-5.34	-2.75
3POIr(mtpy)	498, 486, 509	27.1, 9.2	1.07, 0.87	2.58	0.64	-5.44	-2.86
4POIr(mtpy)	523, 517, 534	45.5, 58.4	1.24, 1.08	2.53	0.53	-5.33	-2.80

^aMeasured in CH₂Cl₂ solution (10⁻⁵ M) at 298 K. ^bMeasured in CH₂Cl₂ solution (10⁻⁵ M) at 77 K. ^cMeasured in the neat film. ^dOptical band gap. ^eMeasured by CV with ferrocene as the standard. ^fCalculated from the onset oxidation potentials of the complexes. ^gEstimated by using the empirical equation of $E_{\text{LUMO}} = E_{\text{HOMO}} + E_{\text{g}}$.

cell assemblies. A silver wire was used as an Ag/Ag⁺ quasi reference electrode, a platinum wire was used as the counter electrode, and a glassy carbon electrode was used as a working electrode. Tetrabutylammonium-hexafluorophosphate (0.1 M) was selected as the supporting electrolyte. At the end of each experiment, ferrocene was selected as the internal standard.

Device Fabrication and Characterization. Organic layers were fabricated by vacuum evaporation onto patterned indium–tin-oxide (ITO)-coated glass substrates with a sheet resistance of 20 Ω per square. All of the complexes were vacuum-deposited without any decomposition. A shadow mask was used to define the cathode and make four 10 mm² devices on each substrate. The thickness of the organic layers and metal was measured in situ with a quartz oscillator. The EL spectra of the devices have been measured on an Ocean Optics Maya 2000-PRO spectrophotometer. All of the measurements were performed at room temperature under ambient conditions.

RESULTS AND DISCUSSION

Photophysical Properties. The UV–vis absorption and PL spectra of these complexes in CH₂Cl₂ (10⁻⁵ M) are depicted in Figure 2a, and the corresponding data are showed in Table 1. In common with most iridium(III) complexes, the absorption spectra mainly consist of two regions: the shorter wavelength (<380 nm) absorptions, which are primarily due to the spin-allowed ¹ π – π^* transitions of the ligands, and the long wavelength (>400 nm) absorptions in the low-energy region, which can be assigned to mixing among the typical spin-allowed metal-to-ligand charge transitions (¹MLCT) and ligand-to-ligand charge transitions (¹LLCT), together with spin-forbidden ³MLCT, ³LLCT, ³LC transitions facilitated by spin–orbit coupling.^{2a,19} The spin–orbit coupling is enhanced caused not only by the presence of π – π^* and MLCT states but also by the heavy-atom effect of Ir center.²⁰

The PL spectra of these complexes measured in CH₂Cl₂ at room temperature are depicted in Figure 2b. All of the complexes display a distinct vibronic structure, indicating that the ³LC excited state contributed to the emissive excited states. 3CzIr(mtpy) and 4CzIr(mtpy) exhibit nearly identical patterns, with emission peaks at 511 and 504 nm, respectively, with Φ = 12.7% (3CzIr(mtpy)) and 10.3% (4CzIr(mtpy)). Additionally, 3POIr(mtpy) and 4POIr(mtpy) are intensely luminescent, with maxima at 498 and 523 nm, respectively, and Φ = 27.1% (3POIr(mtpy)) and 45.5% (4POIr(mtpy)). Typical of other similar Ir(III) complexes upon cooling to 77 K, the spectra become more well-resolved, and the emission maxima blue-shift to 500, 500, 486, and 517 nm. The hypsochromic shifts observed mainly originated from the solvent reorganization in a fluid solution at low temperature, which stabilized the charge-transfer states prior to emission.^{11b,20b,21} Considering the apparent shift in 77 K, we speculate that both the ³MLCT and ³LLCT characters are also

involved in the excited state of these complexes.²² In view of the above analysis, it is believed that their emission should originate from the admixture of ³MLCT, ³LLCT, and ³LC characters.

The emission lifetimes of the complexes are measured to be 0.38, 0.87, 1.07, and 1.24 μs , respectively, which fall into the microsecond timescale. The relative shorter lifetimes of the complexes were expected to increase spin-state mixing, leading to effective intersystem crossing from the singlet to the triplet state.^{20b,23} In the PL spectra of spin-coated neat films, all complexes exhibit obvious red-shifts by ca. 12–15 nm compared to those in solution, probably as a result of the molecular aggregation and TTA in the solid state.²⁴

Theoretical Calculations. Figure 3 shows orbital distributions of the highest occupied molecular orbital (HOMO) and

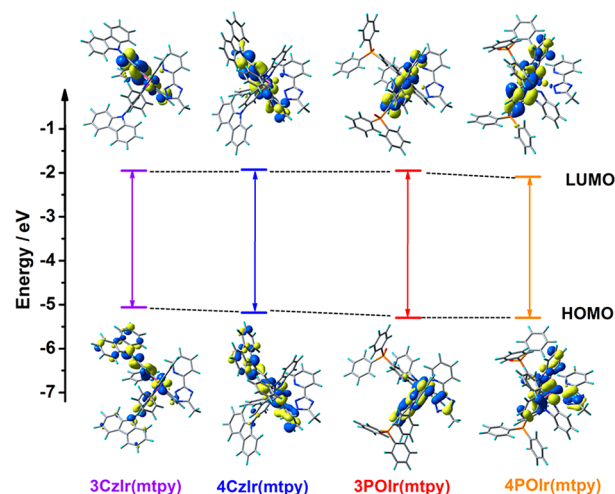


Figure 3. Contours and contributions of the frontier molecular orbitals of studied iridium(III) complexes.

lowest unoccupied molecular orbital (LUMO) energy levels and optimized molecular structures of the two different series. In the case of Cz-based series, the HOMOs contribute mainly from the d orbitals of the iridium atom and the cyclometalated ligand, while the LUMOs distribute mainly at one of the phenylbenzimidazole moieties. For Ph₂PO-based series, the HOMOs contribute mainly from the d orbitals of the iridium atom and the phenylbenzimidazole of one main ligand, with there being a small distribution from the ancillary ligand. As shown in Table S1, the T₁ states of 3CzIr(mtpy) and 4CzIr(mtpy) originate from HOMO → LUMO (80%) and HOMO → LUMO (86%), while 3POIr(mtpy) and 4POIr(mtpy) both originate from HOMO → LUMO (87%). It is conjectured that the mixture of the ³MLCT, ³LC, and ³LLCT

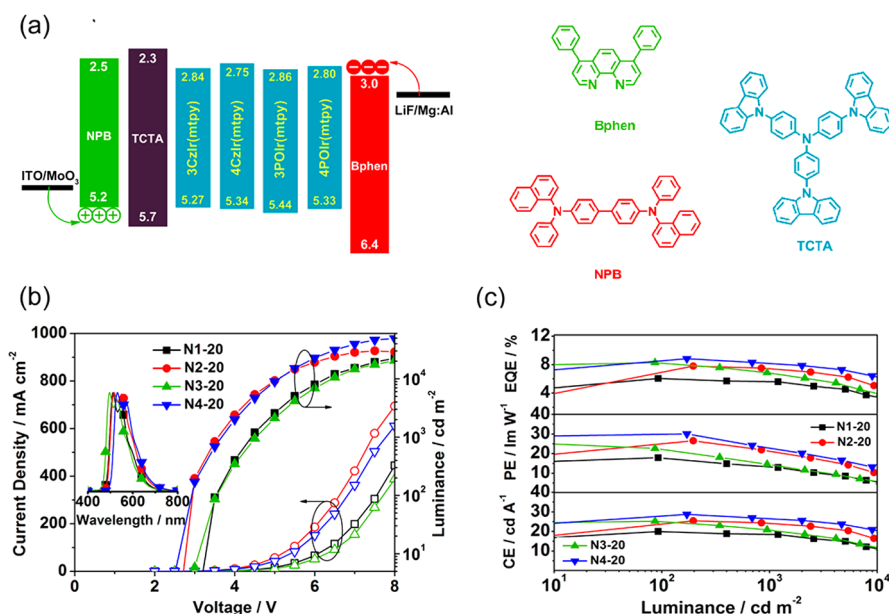


Figure 4. (a) Energy level diagram of nondoped devices N1-20–N4-20 and the chemical structures of employed materials. (b) Current density–voltage–luminance characteristics and EL spectra (inset) of devices N1-20–N4-20. (c) Efficiency–luminance curves of devices N1-20–N4-20 based on 3CzIr(mtpy), 4CzIr(mtpy), 3POIr(mtpy), and 4POIr(mtpy).

transition characters contributed to their emissions. In addition, the differences in electron density between T_1 and the ground state S_0 for these complexes obviously confirm the transition characters mentioned above (see Figure S5).

Electrochemical Properties. The electrochemical properties of these complexes are probed by the cyclic voltammetry (CV), and the relevant electrochemical dates are listed in Table 1. The HOMO energy levels of the complexes were measured by the onset oxidation potentials as -5.27 , -5.34 , -5.44 , and -5.33 eV, respectively. The LUMO energy levels of -2.84 (3CzIr(mtpy)), -2.75 (4CzIr(mtpy)), -2.86 (3POIr(mtpy)), and -2.80 eV (4POIr(mtpy)) were estimated according to the HOMO energy levels and optical band gaps (E_g).⁴ Because of the electron-withdrawing ability of the diphenylphosphoryl group (Ph_2PO) in ligand HPBI, 3POIr(mtpy) and 4POIr(mtpy) showed lower HOMO levels of -5.44 and -5.33 eV relative to 3CzIr(mtpy) (-5.27 eV) and 4CzIr(mtpy) (-5.34 eV).

Device Performance. To understand the electroluminescent properties of these complexes, we fabricated nondoped devices N1-20 (3CzIr(mtpy)), N2-20 (4CzIr(mtpy)), N3-20 (3POIr(mtpy)), and N4-20 (4POIr(mtpy)) with 20 nm thickness of EML, using these carbazole (Cz)- and diphenylphosphoryl (Ph_2PO)-based iridium complexes as the phosphors. A nondoped device with a parent Ir(III) complex was also fabricated as a reference device, namely, N-20. The structure of the fabricated devices as follows: ITO/MoO₃ (3 nm)/NPB (35 nm)/TCTA (5 nm)/Ir complexes (20 nm)/Bphen (40 nm)/LiF (0.5 nm)/Mg:Ag (120 nm, 15:1), in which MoO₃ acts as the hole-injecting layer (HIL), and LiF as an electron-injecting layer (EIL). 4,4-Bis(N-(1-naphthyl)-N-phenylamino)-biphenyl (NPB) was used as the hole-transporting layer (HTL), and 4,7-diphenyl-1,10-phenanthroline (Bphen) was used as the electron-transporting layer (ETL), while the present complexes alone were used as the EML. The energy level diagrams of the device and molecular structures of materials employed are displayed in Figure 4a. From the energy level diagrams, there is a large energy-injection barrier between

4,4',4''-tris(N-carbazolyl)triphenylamine (TCTA) and the emitters (about 0.26–0.43 eV), but TCTA mainly acts as a buffer gradient to facilitate hole injection and block electrons, resulting in a better confinement of excitons in the emission layers and thus improving device performance. The electroluminescence (EL) spectra of devices N1-20–N4-20 at a driving voltage of 5 V are depicted in Figure 4b (inset). The maxima EL emission of the nondoped devices using 3CzIr(mtpy), 4CzIr(mtpy), 3POIr(mtpy), 4POIr(mtpy), and (pbi)₂Ir(mtpy), appear at 513, 517, 496, 532, and 511 nm, respectively. In each case, the EL spectrum is almost coincident with the PL spectrum of the corresponding complex and indicates that the EL and PL spectra originate from the decay of singlet excitons, and the formation of detrimental excimers or exciplexes is effectively suppressed.

The current density–voltage–luminance (J – V – L) characteristics are shown in Figure 4b. The devices exhibit low turn-on voltages (estimated at the brightness of 1 cd m⁻²) of 3.0 V (N1-20), 2.5 V (N2-20), 2.6 V (N3-20), and 2.1 V (N4-20). In addition, they show very low driving voltages at the practical brightness of 100 cd m⁻² and 1000 cd m⁻² for display and lighting. The driving voltages for 100 cd m⁻² and 1000 cd m⁻² were as low as 3.5/4.4, 2.8/3.6, 3.5/4.5, 2.8/3.6 V, respectively. The maxima brightness (L_{max}) of devices N1-20–N4-20 can be as high as 23 258, 30 263, 21 464, and 49 026 cd m⁻², which are far higher than that of control device N-20 (7331 cd m⁻²).

All of the devices exhibit attractive performance with low driving voltages and enhanced luminescence in each case. We can surmise that probably the Cz/Ph₂PO groups not only act as bulky building units to suppress the TTA effect but also play a role in modification of charge-carrier transport characters, so we investigated the J – V characteristics of single-carrier devices to estimate their intrinsic charge-transport process in EML. The configurations of hole-only and electron-only devices are ITO/MoO₃ (3 nm)/NPB (40 nm)/Ir complexes (20 nm)/NPB (40 nm)/MoO₃ (3 nm)/Ag (120 nm) and ITO/LiF (0.5 nm)/Bphen (40 nm)/Ir complexes (20 nm)/Bphen (40 nm)/LiF (0.5 nm)/Ag (120 nm), respectively. For the hole-only devices,

MoO₃ (LUMO = −2.3 eV) was used to block the electron injection from Ag (−4.7 eV), corresponding to a large energy-injection barrier of 2.4 eV. In the electron-only devices, LiF (HOMO = −5.9) was used to block the hole injection from ITO (−4.8 eV), corresponding to a large energy-injection barrier of 1.1 eV.²⁵ As shown in Figure 5, all of the single-carrier

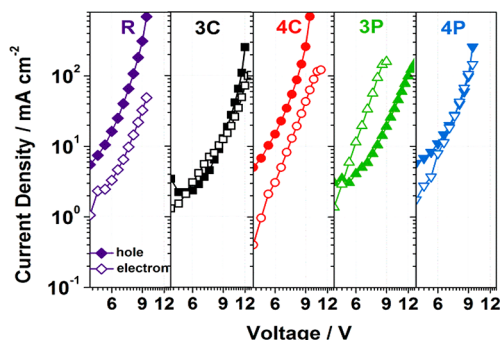


Figure 5. Current density–voltage characteristics of the single-carrier devices (solid for hole-only and hollow for electron-only) based on 3C-3CzIr(mtpy), 4C-4CzIr(mtpy), 3P-3POIr(mtpy), and 4P-4POIr(mtpy) in comparison with that of R-(pbi)₂Ir(mtpy).

devices show significant currents, indicating superiority in charge-carrier mobility. It is also noted that the electron-transporting ability of Cz/Ph₂PO-containing complexes is stronger than that of the parent complex (pbi)₂Ir(mtpy). It is known to be a plausible deduction that conventional devices are almost hole-predominant devices.²⁶ The enhancement of electron transport will facilitate the injection and transport of electrons, broaden the recombination zone, and balance charge flux, particularly for the nondoped devices, which is beneficial for suppressing TTA and TPQ (triplet–polaron quenching) inside the EML through reducing exciton density and excess charges.²⁷ These could explain why the CzIr(mtpy) and

POIr(mtpy)-based devices achieved lower driving voltages, higher current density, and luminescence.

Figure 4c revealed the CE and PE as functions of luminance for these devices. Devices N1-20 and N2-20, based on Cz-containing complexes, displayed good performance, with maxima CE of 19.9 and 25.4 cd A^{−1}, and maxima PE of 17.9 and 26.6 lm W^{−1}. Ph₂PO-containing complexes endowed devices N3-20 and N4-20 with better performance, maxima CE of 25.2 and 28.7 cd A^{−1}, and maxima PE of 22.6 and 30.1 lm W^{−1}. These start-of-the-art efficiencies are almost 2-fold greater than those of the reference device (13.1 cd A^{−1}, 13.7 lm W^{−1}). This significant enhancement should be attributed mainly to its balanced carrier transport induced by the functional units, as revealed by the characteristics of their single-carrier devices. Inspiringly, at a practically high brightness of 1000 cd m^{−2}, their efficiency roll-offs are only 7.0% (N1-20), 4.7% (N2-20), 17.9% (N3-20), and 7.3% (N4-20) for CE, all of which are much lower than that of reference device (31.3%). The results indicate that introducing the Cz/Ph₂PO moieties could effectively suppress the intermolecular aggregation due to the large steric hindrance. In addition, its more balanced carrier transport result in a broader distribution of the recombination zone and efficient confinement of the triplet excitons generated within the EML. These therefore increase the overall device efficiency in many cases. To the best of our knowledge, these are good results for green-emitting PHOLEDs by use of vacuum-evaporation techniques (see Table S2).

To shed light on further optimization of device performance, we changed the thickness of the EML from 20 to 10 nm for the purpose of reducing the self-quenching effect. Nondoped devices N1-10–N4-10 were fabricated with a conventional configuration of ITO/MoO₃ (3 nm)/NPB (35 nm)/TCTA (5 nm)/Ir complexes (10 nm)/Bphen (40 nm)/LiF (0.5 nm)/Mg:Ag (120 nm, 15:1) (as shown in Figure 6a), where the materials employed here are kept unchanged from those used in the analysis of 20 nm thick EML. For comparison, the control device N-10 with parent Ir(III) complex as the EML

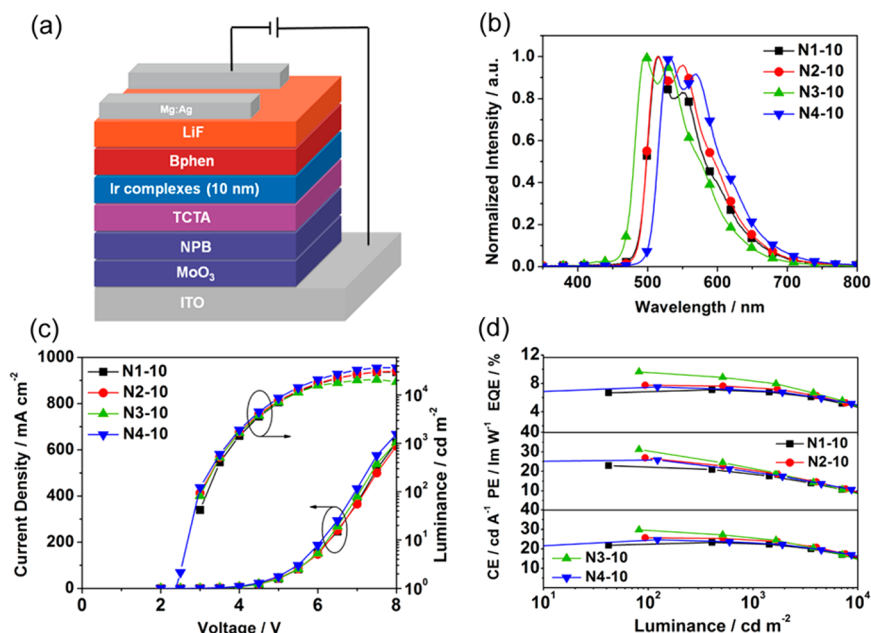


Figure 6. (a) Schematic diagram of EL device configurations. (b) EL spectra of devices with 10 nm thickness of EML (at 5 V). (c) Current density–voltage–luminance characteristics of devices N1-10–N4-10. (d) Efficiency–luminance curves of devices N1-10–N4-10.

Table 2. Summary of the EL Performance of the Devices

device	$V_{\text{turn-on}}^{a,b,c}$ (V)	L_{max}^d (cd m ⁻² , V)	CE ^{d,c} (cd A ⁻¹)	PE ^{d,c} (lm W ⁻¹)	EQE (%)	λ_{EL} (nm)	CIE[(x, y), V]
N-20	2.6, 3.3, 4.3	7331, 7.5	13.1, 9.0	13.7, 6.5	4.1	511	(0.35, 0.57), 5
N1-20	3.0, 3.5, 4.4	23 258, 8.5	19.9, 18.5	17.9, 13.5	6.0	513	(0.35, 0.58), 5
N2-20	2.5, 2.8, 3.6	30 263, 7.5	25.4, 24.2	26.6, 21.2	7.8	517	(0.38, 0.58), 5
N3-20	2.6, 3.5, 4.5	21 646, 8.5	25.2, 20.7	22.6, 14.4	8.3	496	(0.31, 0.55), 5
N4-20	2.1, 2.8, 3.6	49 026, 8.0	28.7, 26.6	30.1, 22.7	8.3	532	(0.42, 0.56), 5
N-10	2.5, 3.1, 4.1	5193, 6.5	11.1, 6.3	11.6, 4.8	3.5	511	(0.35, 0.57), 5
N1-10	2.5, 3.6, 4.7	29 697, 7.5	23.3, 22.7	20.9, 18.9	7.1	515	(0.36, 0.58), 5
N2-10	2.5, 3.0, 3.7	31 106, 8.0	25.7, 24.5	26.9, 20.4	7.7	514	(0.37, 0.58), 5
N3-10	2.5, 3.0, 3.7	20 761, 7.5	29.7, 25.6	31.1, 20.9	9.6	496	(0.30, 0.55), 5
N4-10	2.2, 2.9, 3.6	36 701, 8.0	24.7, 23.3	25.8, 19.9	7.5	532	(0.42, 0.56), 5

^aThe voltages estimated at 1 cd m⁻². ^bMeasured at 100 cd m⁻². ^cMeasured at 1000 cd m⁻². ^dMaximum values of the devices.

was also adopted under the same conditions. As shown by the EL spectra in Figure 6b, all of the devices exhibited yellow-green light with an emission peak at 515 nm and CIE coordinates of (0.36, 0.58) for N1-10, an emission peak at 514 nm and CIE coordinates of (0.37, 0.58) for N2-10, an emission peak at 496 nm and CIE coordinates of (0.30, 0.55) for N3-10, and an emission peak at 532 nm and CIE coordinates of (0.42, 0.56) for N4-10.

The J - V - L characteristics and efficiencies versus luminance curves of these devices are depicted in Figure 6, and the key EL data are summarized in Table 2. All devices display low turn-on voltage, for instance, 2.5 V for N1-10, 2.5 V for N2-10, 2.5 V for N3-10, and 2.2 V for N4-10. Also, similar to the results mentioned above, they show very low driving voltages at high luminances of 100 cd m⁻² and 1000 cd m⁻². Devices N1-10 and N2-10, based on Cz-containing complexes, show a much better performance ($L_{\text{max}} = 29\,697$ cd m⁻², CE = 23.3 cd A⁻¹, and PE = 20.9 lm W⁻¹ for N1-10, $L_{\text{max}} = 31\,106$ cd m⁻², CE = 25.7 cd A⁻¹, and PE = 26.9 lm W⁻¹ for N2-10) than that of the control device ($L_{\text{max}} = 5193$ cd m⁻², CE = 11.1 cd A⁻¹, and PE = 11.6 lm W⁻¹). Similarly, devices N3-10 and N4-10, based on Ph₂PO-containing complexes, exhibit excellent efficiencies with $L_{\text{max}} = 20\,761$ cd m⁻², CE = 29.7 cd A⁻¹, and PE = 31.1 lm W⁻¹ for N3-10, $L_{\text{max}} = 36\,701$ cd m⁻², CE = 24.7 cd A⁻¹, and PE = 25.8 lm W⁻¹ for N4-10, which are almost 3 times of those of the control device. Owing to the low driving voltages, the maximum PE of Ph₂PO-based devices are even higher than their CE, revealing the more effective injection and transport of charges.^{22b,28} Alternatively, it is worth noting that all of the devices showed little efficiency roll-off as the luminance increased. At a high luminance of 1000 cd m⁻², their CE remained as 22.7, 24.5, 25.6, and 23.3 cd A⁻¹, corresponding to reduced efficiency roll-offs of 2.6, 4.7, 13.8, and 5.7%, respectively. The maximum efficiency of the reference device is remarkably decreased to 6.3 cd A⁻¹, accompanied by worse roll-off of 43.2% at 1000 cd m⁻². The excellent EL efficiencies and the improved stability of efficiency should be mainly due to the large steric hindrance caused by the functional moieties, which could partly prevent the formation of excimers or exciplexes and avoid significant TTA and nonemissive pathways caused by intermolecular excited-state interactions.^{2c} Also, the remarkably improved electron mobility of the CzIr(mtpy) and POIr(mtpy) can facilitate carrier flux balance in EML with respect to hole-predominant devices, which further reduced TTA-induced efficiency roll-off.

The success of Cz/Ph₂PO-containing complexes in yellow-green emitting devices with superior EL performance is ascribed to large steric hindrance and balanced charge transport

induced by functional moieties, manifesting the merits of the synthetically versatile strategy. Although significant advances have been achieved in this field, it is believed that better EL data could be obtained through rational molecular design and further device optimization. Herein, we provided a general design strategy to enhance EL performance. We anticipate that the good relationship between molecular structures and device performances obtained will offer excellent support for designing efficient phosphorescence Ir(III) complexes containing an HPBI-cyclometalated ligand and corresponding nondoped devices.

CONCLUSIONS

In summary, we have designed and synthesized four yellow-green phosphorescent emitters, 3CzIr(mtpy), 4CzIr(mtpy), 3POIr(mtpy), and 4POIr(mtpy), consisting of functional moieties (Cz and Ph₂PO) substituted at different positions of HPBI and investigated their applications in nondoped OLEDs. It was shown that, as steric-hindrance-inducing groups, Cz and Ph₂PO could efficiently suppress intermolecular interaction and reduce self-quenching effects. By introducing the functional groups, charge-carrier transportation characters were nicely modified. As a result, all nondoped devices exhibited the state-of-the-art performance and reduced efficiency roll-off, which are much higher than that of the control device. Nondoped device N3-10, based on 3POIr(mtpy), showed excellent EL efficiencies, including the maximum CE of 29.7 cd A⁻¹ and the maximum PE of 31.1 lm W⁻¹, which are almost 3 times than that of the unfunctionalized counterpart. This work manifested the great potential of these functional materials as high performance EMLs for nondoped OLEDs, and provided an easy molecular design strategy to develop efficient phosphors for optical devices.

ASSOCIATED CONTENT

Supporting Information

The Supporting Information is available free of charge on the ACS Publications website at DOI: 10.1021/acs.inorgchem.7b01516.

Supplemental schemes, figures, and calculated energy levels of the lower-lying transitions of all complexes (PDF)

AUTHOR INFORMATION

Corresponding Authors

*G.-G.S.: Fax: +86-431-85684009; Tel.: +86-431-85099108; E-mail: shangg187@nenu.edu.cn

*W.-F.X.: Tel: +86-13844907598; E-mail: xiewf@jlu.edu.cn

*Z.-M.S.: E-mail: zmsu@nenu.edu.cn

ORCID

Hai-Zhu Sun: 0000-0002-5113-8267

Zhong-Min Su: 0000-0002-3342-1966

Notes

The authors declare no competing financial interest.

ACKNOWLEDGMENTS

The authors gratefully acknowledge the financial support from National Natural Science Foundation of China (21303012, 21273030, 51203017, 21131001, and 61474054), 973 Program (2013CB834801), and the Science and Technology Development Planning of Jilin Province 20130204025GX.

REFERENCES

- (1) (a) Baldo, M. A.; O'Brien, D. F.; You, Y.; Shoustikov, A.; Sibley, S.; Thompson, M. E.; Forrest, S. R. Highly efficient phosphorescent emission from organic electroluminescent devices. *Nature* **1998**, *395*, 151–154. (b) Reineke, S.; Lindner, F.; Schwartz, G.; Seidler, N.; Walzer, K.; Lussem, B.; Leo, K. White organic light-emitting diodes with fluorescent tube efficiency. *Nature* **2009**, *459*, 234–238. (c) Fan, C.; Li, Y.; Yang, C.; Wu, H.; Qin, J.; Cao, Y. Phosphoryl/Sulfonyl-Substituted Iridium Complexes as Blue Phosphorescent Emitters for Single-Layer Blue and White Organic Light-Emitting Diodes by Solution Process. *Chem. Mater.* **2012**, *24*, 4581–4587.
- (2) (a) Lamansky, S.; Djurovich, P.; Murphy, D.; Abdel-Razzaq, F.; Lee, H.-E.; Adachi, C.; Burrows, P. E.; Forrest, S. R.; Thompson, M. E. Highly Phosphorescent Bis-Cyclometalated Iridium Complexes: Synthesis, Photophysical Characterization, and Use in Organic Light Emitting Diodes. *J. Am. Chem. Soc.* **2001**, *123*, 4304–4312. (b) Ding, J.; Wang, B.; Yue, Z.; Yao, B.; Xie, Z.; Cheng, Y.; Wang, L.; Jing, X.; Wang, F. Bifunctional green iridium dendrimers with a "self-host" feature for highly efficient nondoped electrophosphorescent devices. *Angew. Chem., Int. Ed.* **2009**, *48*, 6664–6666. (c) You, Y.; Nam, W. Photofunctional triplet excited states of cyclometalated Ir(III) complexes: beyond electroluminescence. *Chem. Soc. Rev.* **2012**, *41*, 7061–7084.
- (3) Orselli, E.; Kottas, G. S.; Konradsson, A. E.; Coppo, P.; Frohlich, R.; De Cola, L.; van Dijken, A.; Buchel, M.; Borner, H. Blue-Emitting Iridium Complexes with Substituted 1,2,4-Triazole Ligands: Synthesis, Photophysics, and Devices. *Inorg. Chem.* **2007**, *46*, 11082–11093.
- (4) (a) Qin, T.; Ding, J.; Wang, L.; Baumgarten, M.; Zhou, G.; Müllen, K. A Divergent Synthesis of Very Large Polyphenylene Dendrimers with Iridium(III) Cores: Molecular Size Effect on the Performance of Phosphorescent Organic Light-Emitting Diodes. *J. Am. Chem. Soc.* **2009**, *131*, 14329–14336. (b) Wang, Y.; Lu, Y.; Gao, B.; Wang, S.; Ding, J.; Wang, L.; Jing, X.; Wang, F. Self-Host Blue-Emitting Iridium Dendrimer Containing Bipolar Dendrons for Nondoped Electrophosphorescent Devices with Superior High-Brightness Performance. *ACS Appl. Mater. Interfaces* **2016**, *8*, 29600–29607.
- (5) (a) Xue, K.; Sheng, R.; Duan, Y.; Chen, P.; Chen, B.; Wang, X.; Duan, Y.; Zhao, Y. Efficient non-doped monochrome and white phosphorescent organic light-emitting diodes based on ultrathin emissive layers. *Org. Electron.* **2015**, *26*, 451–457. (b) Tsai, W. L.; Huang, M. H.; Lee, W. K.; Hsu, Y. J.; Pan, K. C.; Huang, Y. H.; Ting, H. C.; Sarma, M.; Ho, Y. Y.; Hu, H. C.; Chen, C. C.; Lee, M. T.; Wong, K. T.; Wu, C. C. A versatile thermally activated delayed fluorescence emitter for both highly efficient doped and non-doped organic light emitting devices. *Chem. Commun.* **2015**, *51*, 13662–13665. (c) Tang, C.; Liu, F.; Xia, Y.-J.; Lin, J.; Xie, L.-H.; Zhong, G.-Y.; Fan, Q.-L.; Huang, W. Fluorene-substituted pyrenes-Novel pyrene derivatives as emitters in nondoped blue OLEDs. *Org. Electron.* **2006**, *7*, 155–162. (d) Meng, L.; Wang, H.; Wei, X.; Liu, J.; Chen, Y.; Kong, X.; Lv, X.; Wang, P.; Wang, Y. Highly Efficient Nondoped Organic Light Emitting Diodes Based on Thermally Activated Delayed Fluorescence Emitter with Quantum-Well Structure. *ACS Appl. Mater. Interfaces* **2016**, *8*, 20955–20961.
- (6) (a) Huang, T. H.; Lin, J. T.; Chen, L. Y.; Lin, Y. T.; Wu, C. C. Dipolar Dibenzothiophene S,S-Dioxide Derivatives Containing Diarylamine: Materials for Single-Layer Organic Light-Emitting Devices. *Adv. Mater.* **2006**, *18*, 602–606. (b) Shi, H. P.; Xin, D. H.; Gu, X. G.; Zhang, P. F.; Peng, H. R.; Chen, S. M.; Lin, G. W.; Zhao, Z. J.; Tang, B. Z. The synthesis of novel AIE emitters with the triphenylethene-carbazole skeleton and para-/meta-substituted arylboron groups and their application in efficient non-doped OLEDs. *J. Mater. Chem. C* **2016**, *4*, 1228–1237.
- (7) Zhang, Y.; Lai, S.-L.; Tong, Q.-X.; Lo, M.-F.; Ng, T.-W.; Chan, M.-Y.; Wen, Z.-C.; He, J.; Jeff, K.-S.; Tang, X.-L.; Liu, W.-M.; Ko, C.-C.; Wang, P.-F.; Lee, C.-S. High Efficiency Nondoped Deep-Blue Organic Light Emitting Devices Based on Imidazole- π -triphenylamine Derivatives. *Chem. Mater.* **2012**, *24*, 61–70.
- (8) Liu, Y.; Ye, K.; Fan, Y.; Song, W.; Wang, Y.; Hou, Z. Amidinate-ligated iridium(III) bis(2-pyridyl)phenyl complex as an excellent phosphorescent material for electroluminescence devices. *Chem. Commun.* **2009**, 3699–3701.
- (9) (a) Cao, H.; Shan, G.; Wen, X.; Sun, H.; Su, Z.; Zhong, R.; Xie, W.; Li, P.; Zhu, D. An orange iridium(III) complex with wide-bandwidth in electroluminescence for fabrication of high-quality white organic light-emitting diodes. *J. Mater. Chem. C* **2013**, *1*, 7371–7379. (b) Shan, G. G.; Li, H. B.; Sun, H. Z.; Cao, H. T.; Zhu, D. X.; Su, Z. M. Enhancing the luminescence properties and stability of cationic iridium(III) complexes based on phenylbenzimidazole ligand: a combined experimental and theoretical study. *Dalton Trans.* **2013**, *42*, 11056–11065. (c) Cao, H.-T.; Shan, G.-G.; Yin, Y.-M.; Sun, H.-Z.; Wu, Y.; Xie, W.-F.; Su, Z.-M. Modification of iridium(III) complexes for fabrication of high-performance non-doped organic light-emitting diode. *Dyes Pigm.* **2015**, *112*, 8–16. (d) Mao, H.-T.; Zang, C.-X.; Wen, L. L.; Shan, G.-G.; Sun, H.-Z.; Xie, W.-F.; Su, Z.-M. Ir(III) Phosphors Modified with Fluorine Atoms in Pyridine-1,2,4-triazolyl Ligands for Efficient OLEDs Possessing Low-Efficiency Roll-off. *Organometallics* **2016**, *35*, 3870–3877.
- (10) Wen, L.-L.; Yu, J.; Sun, H.-Z.; Shan, G.-G.; Zhao, K.-Y.; Xie, W.-F.; Su, Z.-M. Simple molecular structure design of iridium(III) complexes: Achieving highly efficient non-doped devices with low efficiency roll-off. *Org. Electron.* **2016**, *35*, 142–150.
- (11) (a) Xu, H.; Chen, R.; Sun, Q.; Lai, W.; Su, Q.; Huang, W.; Liu, X. Recent progress in metal-organic complexes for optoelectronic applications. *Chem. Soc. Rev.* **2014**, *43*, 3259–3302. (b) Zhou, G.; Ho, C.-L.; Wong, W.-Y.; Wang, Q.; Ma, D.; Wang, L.; Lin, Z.; Marder, T. B.; Beeby, A. Manipulating Charge-Transfer Character with Electron-Withdrawing Main-Group Moieties for the Color Tuning of Iridium Electrophosphors. *Adv. Funct. Mater.* **2008**, *18*, 499–511. (c) Yang, C. L.; Zhang, X. W.; You, H.; Zhu, L. Y.; Chen, L. Q.; Zhu, L. N.; Tao, Y. T.; Ma, D. G.; Shuai, Z. G.; Qin, J. G. Tuning the Energy Level and Photophysical and Electroluminescent Properties of Heavy Metal Complexes by Controlling the Ligation of the Metal with the Carbon of the Carbazole Unit. *Adv. Funct. Mater.* **2007**, *17*, 651–661. (d) Zhu, M.; Li, Y.; Miao, J.; Jiang, B.; Yang, C.; Wu, H.; Qin, J.; Cao, Y. Multifunctional homoleptic iridium(III) dendrimers towards solution-processed nondoped electrophosphorescence with low efficiency roll-off. *Org. Electron.* **2014**, *15*, 1598–1606.
- (12) (a) Ding, J.; Lü, J.; Cheng, Y.; Xie, Z.; Wang, L.; Jing, X.; Wang, F. Solution-Processible Red Iridium Dendrimers based on Oligocarbazole Host Dendrons: Synthesis, Properties, and their Applications in Organic Light-Emitting Diodes. *Adv. Funct. Mater.* **2008**, *18*, 2754–2762. (b) Pu, Y.-J.; Iguchi, N.; Aizawa, N.; Sasabe, H.; Nakayama, K.-i.; Kido, J. fac-Tris(2-phenylpyridine)iridium (III)s, covalently surrounded by six bulky host dendrons, for a highly efficient solution-processed organic light emitting device. *Org. Electron.* **2011**, *12*, 2103–2110.
- (13) Kan, W. J.; Zhu, L. P.; Wei, Y.; Ma, D. G.; Sun, M. Z.; Wu, Z. B.; Huang, W.; Xu, H. Phosphine oxide-jointed electron transporters for the reduction of interfacial quenching in highly efficient blue PHOLEDs. *J. Mater. Chem. C* **2015**, *3*, 5430–5439.

- (14) Chen, T.-R. Synthesis, structure, and field-effect property of 2-(benzimidazol-2-yl) quinoline. *Mater. Lett.* **2005**, *59*, 1050–1052.
- (15) Frisch, M. J.; Trucks, G. W.; Schlegel, H. B.; Scuseria, G. E.; Robb, M. A.; Cheeseman, J. R.; Scalmani, G.; Barone, V.; Mennucci, B.; Petersson, G. A.; Nakatsuji, H.; Caricato, M.; Li, X.; Hratchian, H. P.; Izmaylov, A. F.; Bloino, J.; Zheng, G.; Sonnenberg, J. L.; Hada, M.; Ehara, M.; Toyota, K.; Fukuda, R.; Hasegawa, J.; Ishida, M.; Nakajima, T.; Honda, Y.; Kitao, O.; Nakai, H.; Vreven, T.; Montgomery, J. A., Jr.; Peralta, J. E.; Ogliaro, F.; Bearpark, M.; Heyd, J. J.; Brothers, E.; Kudin, K. N.; Staroverov, V. N.; Keith, T.; Kobayashi, R.; Normand, J.; Raghavachari, K.; Rendell, A.; Burant, J. C.; Iyengar, S. S.; Tomasi, J.; Cossi, M.; Rega, N.; Millam, J. M.; Klene, M.; Knox, J. E.; Cross, J. B.; Bakken, V.; Adamo, C.; Jaramillo, J.; Gomperts, R.; Stratmann, R. E.; Yazyev, O.; Austin, A. J.; Cammi, R.; Pomelli, C.; Ochterski, J. W.; Martin, R. L.; Morokuma, K.; Zakrzewski, V. G.; Voth, G. A.; Salvador, P.; Dannenberg, J. J.; Dapprich, S.; Daniels, A. D.; Farkas, O.; Foresman, J. B.; Ortiz, J. V.; Cioslowski, J.; Fox, D. J. *Gaussian 09*, Revision A.01; Gaussian, Inc.: Wallingford, CT, 2009.
- (16) Francl, M. M.; Pietro, W. J.; Hehre, W. J.; Binkley, J. S.; Gordon, M. S.; Defrees, D. J.; Pople, J. A. Self-consistent molecular orbital methods. XXIII. A polarization-type basis set for second-row elements. *J. Chem. Phys.* **1982**, *77*, 3654–3665.
- (17) Hay, J. P.; Wadt, W. R. Ab initio effective core potentials for molecular calculations. Potentials for K to Au including the outermost core orbitals. *J. Chem. Phys.* **1985**, *82*, 299–310.
- (18) Peach, M. J.; Williamson, M. J.; Tozer, D. J. Influence of Triplet Instabilities in TDDFT. *J. Chem. Theory Comput.* **2011**, *7*, 3578–3585.
- (19) Nazeeruddin, M. K.; Humphry-Baker, R.; Berner, D.; Rivier, S.; Zuppiroli, L.; Graetzel, M. Highly Phosphorescence Iridium Complexes and Their Application in Organic Light-Emitting Devices. *J. Am. Chem. Soc.* **2003**, *125*, 8790–8797.
- (20) (a) Ho, C. L.; Wong, W. Y.; Zhou, G. J.; Yao, B.; Xie, Z.; Wang, L. Solution-Processible Multi-component Cyclometalated Iridium Phosphors for High-Efficiency Orange-emitting OLEDs and Their Potential Use as White Light Sources. *Adv. Funct. Mater.* **2007**, *17*, 2925–2936. (b) Ho, C.-L.; Wong, W.-Y.; Wang, Q.; Ma, D.; Wang, L.; Lin, Z. A Multifunctional Iridium-Carbazolyl Orange Phosphor for High-Performance Two-Element WOLED Exploiting Exciton-Managed Fluorescence/Phosphorescence. *Adv. Funct. Mater.* **2008**, *18*, 928–937. (c) Wang, Y.; Herron, N.; Grushin, V. V.; LeCloux, D.; Petrov, V. Highly efficient electroluminescent materials based on fluorinated organometallic iridium compounds. *Appl. Phys. Lett.* **2001**, *79*, 449–451. (d) Lee, S.-J.; Park, J.-S.; Song, M.; Shin, I. A.; Kim, Y.-I.; Lee, J. W.; Kang, J.-W.; Gal, Y.-S.; Kang, S.; Lee, J. Y.; Jung, S.-H.; Kim, H.-S.; Chae, M.-Y.; Jin, S.-H. Synthesis and Characterization of Red-Emitting Iridium(III) Complexes for Solution-Processable Phosphorescent Organic Light-Emitting Diodes. *Adv. Funct. Mater.* **2009**, *19*, 2205–2212.
- (21) (a) Tamayo, A. B.; Garon, S.; Sajoto, T.; Djurovich, P. I.; Tsyba, I. M.; Bau, R.; Thompson, M. E. Cationic Bis-cyclometalated Iridium(III) Diimine Complexes and Their Use in Efficient Blue, Green, and Red Electroluminescent Devices. *Inorg. Chem.* **2005**, *44*, 8723–8732. (b) Ho, C. L.; Wong, W. Y.; Gao, Z. Q.; Chen, C. H.; Cheah, K. W.; Yao, B.; Xie, Z. Y.; Wang, Q.; Ma, D. G.; Wang, L. X.; Yu, X. M.; Kwok, H. S.; Lin, Z. Y. Red-Light-Emitting Iridium Complexes with Hole-Transporting 9-Arylcarbazole Moieties for Electrophosphorescence Efficiency/Color Purity Trade-off Optimization. *Adv. Funct. Mater.* **2008**, *18*, 319–331. (c) Zhao, Q.; Li, F.; Liu, S.; Yu, M.; Liu, Z.; Yi, T.; Huang, C. Highly Selective Phosphorescent Chemosensor for Fluoride Based on an Iridium(III) Complex Containing Arylborane Units. *Inorg. Chem.* **2008**, *47*, 9256–9264.
- (22) Wong, W.-Y.; Ho, C.-L. Functional metallophosphors for effective charge carrier injection/transport: new robust OLED materials with emerging applications. *J. Mater. Chem.* **2009**, *19*, 4457–4482.
- (23) (a) Zhu, Y. C.; Zhou, L.; Li, H. Y.; Xu, Q. L.; Teng, M. Y.; Zheng, Y. X.; Zuo, J. L.; Zhang, H. J.; You, X. Z. Highly efficient green and blue-green phosphorescent OLEDs based on iridium complexes with the tetraphenylimidodiphosphate ligand. *Adv. Mater.* **2011**, *23*, 4041–4046. (b) Ho, C. L.; Wang, Q.; Lam, C. S.; Wong, W. Y.; Ma, D.; Wang, L.; Gao, Z. Q.; Chen, C. H.; Cheah, K. W.; Lin, Z. Phosphorescence color tuning by ligand, and substituent effects of multifunctional iridium(III) cyclometalates with 9-arylcarbazole moieties. *Chem. - Asian J.* **2009**, *4*, 89–103.
- (24) (a) He, L.; Duan, L.; Qiao, J.; Wang, R.; Wei, P.; Wang, L.; Qiu, Y. Blue-Emitting Cationic Iridium Complexes with 2-(1*H*-Pyrazol-1-yl)pyridine as the Ancillary Ligand for Efficient Light-Emitting Electrochemical Cells. *Adv. Funct. Mater.* **2008**, *18*, 2123–2131. (b) Shan, G.-G.; Li, H.-B.; Cao, H.-T.; Sun, H.-Z.; Zhu, D.-X.; Su, Z.-M. Influence of alkyl chain lengths on the properties of iridium(III)-based piezochromic luminescent dyes with triazole-pyridine type ancillary ligands. *Dyes Pigm.* **2013**, *99*, 1082–1090.
- (25) Wang, K.; Zhao, F.; Wang, C.; Chen, S.; Chen, D.; Zhang, H.; Liu, Y.; Ma, D.; Wang, Y. High-Performance Red, Green, and Blue Electroluminescent Devices Based on Blue Emitters with Small Singlet-Triplet Splitting and Ambipolar Transport Property. *Adv. Funct. Mater.* **2013**, *23*, 2672–2680.
- (26) (a) Antoniadis, H.; Abkowitz, M. A.; Hsieh, B. R. Carrier deep-trapping mobility-lifetime products in poly(p-phenylene vinylene). *Appl. Phys. Lett.* **1994**, *65*, 2030–2032. (b) Kepler, R. G.; Beeson, P. M.; Jacobs, S. J.; Anderson, R. A.; Sinclair, M. B.; Valencia, V. S.; Cahill, P. A. Electron and hole mobility in tris(8-hydroxyquinolinolato-N1,O8) aluminum. *Appl. Phys. Lett.* **1995**, *66*, 3618–3620.
- (27) (a) Wu, C.; Djurovich, P. I.; Thompson, M. E. Study of Energy Transfer and Triplet Exciton Diffusion in Hole-Transporting Host Materials. *Adv. Funct. Mater.* **2009**, *19*, 3157–3164. (b) Han, T. H.; Choi, M. R.; Woo, S. H.; Min, S. Y.; Lee, C. L.; Lee, T. W. Molecularly controlled interfacial layer strategy toward highly efficient simple-structured organic light-emitting diodes. *Adv. Mater.* **2012**, *24*, 1487–1493. (c) Wang, Z. B.; Helander, M. G.; Liu, Z. W.; Greiner, M. T.; Qiu, J.; Lu, Z. H. Controlling carrier accumulation and exciton formation in organic light emitting diodes. *Appl. Phys. Lett.* **2010**, *96*, 043303.
- (28) (a) He, G.; Pfeiffer, M.; Leo, K.; Hofmann, M.; Birnstock, J.; Pudzich, R.; Salbeck, J. High-efficiency and low-voltage p-i-n electrophosphorescent organic light-emitting diodes with double-emission layers. *Appl. Phys. Lett.* **2004**, *85*, 3911–3913. (b) Zhang, J.; Ding, D.; Wei, Y.; Han, F.; Xu, H.; Huang, W. Multiphosphine-Oxide Hosts for Ultralow-Voltage-Driven True-Blue Thermally Activated Delayed Fluorescence Diodes with External Quantum Efficiency beyond 20%. *Adv. Mater.* **2016**, *28*, 479–485. (c) Li, W.; Li, J.; Liu, D.; Li, D.; Wang, F. Cyanopyridine Based Bipolar Host Materials for Green Electrophosphorescence with Extremely Low Turn-On Voltages and High Power Efficiencies. *ACS Appl. Mater. Interfaces* **2016**, *8*, 21497–21504.